International Journal of Multiphase Flow 35 (2009) 676–688

Contents lists available at ScienceDirect

International Journal of Multiphase Flow

journal homepage: www.elsevier.com/locate/ijmulflow

Fiber suspension flow in a tapered channel: The effect of flow/fiber coupling

Paul J. Krochak [a,*], James A. Olson [a], D. Mark Martinez [b]

[a] The Pulp and Paper Centre, Department of Mechanical Engineering, The University of British Columbia, 2324 Main Mall, Vancouver, BC, Canada V6T 1Z4
[b] Department of Chemical and Biological Engineering, The University of British Columbia, 2360 East Mall, Vancouver, BC, Canada V6T 1Z3

ARTICLE INFO

Article history:
Received 17 September 2008
Received in revised form 4 March 2009
Accepted 7 March 2009
Available online 20 March 2009

Keywords:
Fiber suspension
Two-way coupling
Fiber orientation
Planar contraction

ABSTRACT

A numerical model for predicting the flow and orientation state of semi-dilute, rigid fiber suspensions in a tapered channel is presented. The effect of the two-way flow/fiber coupling is investigated for low Reynolds number flow using the constitutive model of Shaqfeh and Fredrickson. An orientation distribution function is used to describe the local orientation state of the suspension and evolves according to a Fokker–Plank type equation. The planar orientation distribution function is determined along streamlines of the flow and is coupled with the fluid momentum equations through a fourth-order orientation tensor. The coupling term accounts for the two-way interaction and momentum exchange between the fluid and fiber phases. The fibers are free to interact through long range hydrodynamic fiber–fiber interactions which are modeled using a rotary diffusion coefficient, an approach outlined by Folgar and Tucker. Numerical predictions are made for two different orientation states at the inlet to the contraction, namely a fully random and a partially aligned fiber orientation state. Results from these numerical predictions show that the streamlines of the flow are altered and that velocity profiles change from Jeffery–Hamel, to something resembling a plug flow when the fiber phase is considered in the fluid momentum equations. This phenomenon was found when the suspension enters the channel in either a pre-aligned, or in a fully random orientation state. When the suspension enters the channel in an aligned orientation state, fiber orientation is shown to be only marginally changed when the two-way coupling is included. However, significant differences between coupled and uncoupled predictions of fiber orientation were found when the suspension enters the channel in a random orientation state. In this case, the suspension was shown to align much more quickly when the mutual coupling was accounted for and profiles of the orientation anisotropy were considerably different both qualitatively and quantitatively.

1. Introduction

In this work, we investigate the effect of the two-way coupling between the flow field and the orientation state of rigid fiber suspensions flowing through a tapered channel. Flow in the channel is governed by Cauhy's momentum equations for viscous, incompressible, planar, isothermal flow, using the constitutive model of Shaqfeh and Fredrickson (1990) to describe the local stress contribution from the fiber phase. The fiber concentration considered here is semi-dilute, which is be defined mathematically through the following relationship (e.g. Doi and Edwards, 1984):

$$1 \leqslant nL^3 \leqslant \frac{L}{d} \tag{1}$$

where n is the number density of fibers in the suspension, that is, the number of fibers per unit volume, L is the fiber length and d is the fiber diameter. In this study, we consider suspensions with identical properties to those used in the experiments performed by Krochak et al. (2008). These suspensions contained fibers of length $L = 5$ mm, diameter, $d = 0.1$ mm and of concentration $nL^3 = 8$. The fiber aspect ratio, r, that is, the ratio of fiber length, L to its diameter, d, is 50. The Reynolds number, based on the length of the fiber is asymptotically small and based on the inlet channel height is approximately 500.

Controlling the orientation state of fiber suspensions in tapered channel flows is of major interest to papermaking. During papermaking, a semi-dilute fiber suspension flows through a specially shaped duct called a headbox. The first section of the headbox consists of a manifold that sets up a uniform flow across the duct. The flocculated fiber suspension is then fluidized by turbulence created locally from a sudden change in geometry just after the manifold. This is indicated in Fig. 1 as the turbulence generators. The fluidized fiber suspension subsequently passes through a planar contraction called the nozzle, which accelerates the fluid to a high speed and creates a thin planar jet. The jet is typically 10 m wide, 1 cm thick with a mean velocity in excess of 20 m/s. The jet then impinges on a permeable mesh where the water is drained and

* Corresponding author. Tel.: +1 604 822 2813.
E-mail address: krochak@interchange.ubc.ca (P.J. Krochak).

0301-9322/$ - see front matter © 2009 Elsevier Ltd. All rights reserved.
doi:10.1016/j.ijmultiphaseflow.2009.03.005

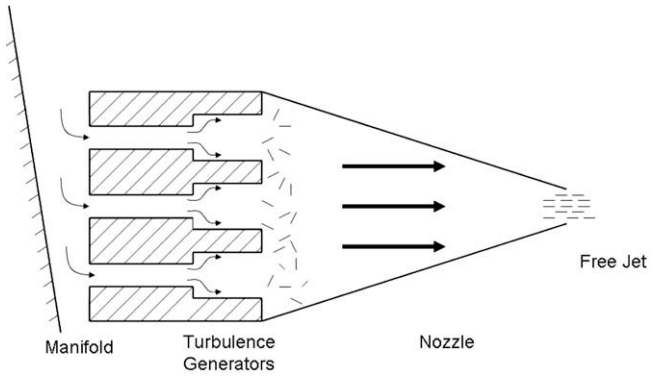

Fig. 1. A generalized industrial headbox.

the paper sheet formed. The orientation distribution of the pulp fibers on the forming mesh plays a fundamental role in determining the strength of the final product.

Fiber orientation in paper depends on a number of different factors, such as the fiber orientation state at the contraction inlet, the concentration of fibers in the suspension, and perhaps most importantly, on the flow field generated after the turbulence generator. Major theoretical developments in fiber suspension rheology have been made over the last two decades. Perhaps most notably, it has been established that the suspension rheology and flow field respond to the orientation state of the suspension (e.g. Batchelor, 1970; Cox, 1970; VerWeyst and Tucker, 2002; Lipscomb and Denn, 1988). The result is a two-way coupling between the fiber orientation state and the underlying flow field. The first to address this issue was Batchelor (1970) who developed a general constitutive equation for the bulk stress in a suspension of rigid, inertialess particles of arbitrary shape in a Newtonian fluid. By representing a single particle in suspension as a distribution of Stokeslets over a line enclosed by the particle body, Batchelor determined expressions for the resultant force required sustaining translational motion and the resultant couple required to sustain rotational motion. Dinh and Armstrong (1984) extended Batchelor's theory to account for the orientation state of elongated particles and its effect on the bulk stress within the suspension. This was accomplished by assuming that the orientation state of the suspension can be completely described by a known orientation distribution function, Ψ, such that the probability of finding fibers oriented between the angles ϕ and $\phi + \partial\phi$ is $\Psi(\phi)\partial\phi$. By linearizing the flow field around the particle they were able to equate Batchelor's constitutive equation to a new constitutive equation; one that is proportional to the fourth-order moment tensor of Ψ. The proportionality constant is referred to as the effective viscosity of the suspension. Shaqfeh and Fredrickson (1990) derived asymptotic expressions for the effective viscosity of dilute and semi-dilute suspensions of rods in a Newtonian fluid. For semi-dilute fiber suspensions, they express the fiber stress as follows:

$$\tau^{\text{fiber}} = \frac{\mu c r^2 \dot{\gamma} : \langle \mathbf{pppp} \rangle}{\ln(1/c) + \ln(\ln(1/c)) + 1.439} \tag{2}$$

where c is the volume fraction of fibers within the suspension which can be related to the concentration parameter, nL^3 as $c = \frac{4\pi n L^3}{3r^2}$; μ is the viscosity of the suspending fluid and $\dot{\gamma}$ is the fluid strain rate tensor, defined as

$$\dot{\gamma} = (\nabla \mathbf{u} + \nabla \mathbf{u}^{\mathbf{T}}) \tag{3}$$

The remaining term that needs to be defined in Eq. (2) is the fourth-order moment of the orientation distribution function Ψ. It is often referred to as the fourth-order orientation tensor and is defined as

$$\langle \mathbf{pppp} \rangle = \int p_i p_j p_k p_l \Psi(\phi)\, d\phi \tag{4}$$

where $\mathbf{p}$ is a unit vector pointing in the direction parallel to the axis of the fiber, that is

$$\mathbf{p} = \begin{bmatrix} \cos\phi \sin\theta \\ \sin\phi \sin\theta \\ \cos\theta \end{bmatrix} \tag{5}$$

where ϕ is the projected angle of the fiber in the xy-plane and θ is the angle between the fiber and the z-axis, see Fig. 2.

The analytic theory of fiber motion in Newtonian flows is also well established. Jeffery's equation of motion (Jeffery, 1922) for a single rigid ellipsoid in an unbounded flow forms the basis for most of this work. For cases above the dilute limit, quantitative relationships between the suspension orientation state and processing conditions have shown that the problem formulation should account for the fact that fibers orient in response to gradients in the flow and disorient in response to hydrodynamic fiber–fiber interactions (e.g. Koch, 1995; Folgar and Tucker, 1984; Rahnama et al., 1995; Altan et al., 1989; Lipscomb and Denn, 1988; Jackson et al., 1985). To help address this issue, Folgar and Tucker (1984) model fiber–fiber interactions as randomly occurring events resulting in a behavior which seemingly mimics a diffusion-type process. In this approach, these authors use an empirically determined rotary diffusion coefficient, D_r, whose value is unknown *a priori* and must be determined through experiment. They proposed, through dimensional analysis, a simple relationship in which D_r is linearly proportional to the magnitude of the rate of strain tensor, $\|\dot{\gamma}\|$. For two dimensional flow in a linear contraction, D_r can be expressed as

$$D_r = C_I \|\dot{\gamma}\| \tag{6}$$

where C_I is traditionally called the interaction coefficient and is related to a number of suspension parameters such as concentration, aspect ratio, and fiber length.

Recently, researchers have been making great efforts to perform 3D fiber orientation predictions for 2D and 3D flows inside complex geometries using a fully coupled model of fiber orientation (e.g. VerWeyst and Tucker, 1999, 2002; Lipscomb and Denn, 1988; Lin and Zhang, 2002). The difficulty with this approach lies in the large computational domain required to resolve both the spatial and orientation domains when directly computing the orientation distribution function. In order to deal with this problem, researchers have had to rely on the use of orientation tensors to predict fiber orientation as opposed to a direct computation of the orientation distribution function (e.g. Jackson et al., 1985; VerWeyst and Tucker, 1999, 2002). The second-order orientation tensor, $\langle \mathbf{pp} \rangle$, for the orientation distribution function, Ψ, contains

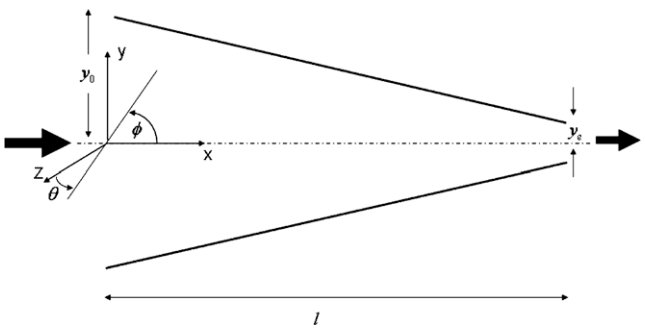

Fig. 2. The orientation of a fiber with respect to flow in a linear contraction. ϕ is the angle of the fiber projected into the xy-plane and the θ is the angle of the fiber with respect to the z-axis.

all the useful information on the orientation state of the suspension. For example, the eigenvectors of $\langle \mathbf{pp} \rangle$ give the principal directions of fiber alignment, while the associated eigenvalues give the magnitude of fiber alignment in that direction (e.g. Advani and Tucker, 1987). The problem with modeling $\langle \mathbf{pp} \rangle$, however, is that the system of equations is not closed therefore a closure approximation is always needed (e.g. Advani and Tucker, 1987, 1990). A further complication to the problem is that the best known closure approximations rely on some *a priori* knowledge of the orientation distribution itself (e.g. Cintra and Tucker, 1995; Chung and Kwon, 2001), either experimental data or a direct computation of the orientation distribution function. This makes stand alone predictions using this method extremely difficult. Parsheh et al. (2005) evaluated the performance of existing closure models with application to accelerating flows by experimentally measuring the fiber orientation distribution along the centerline of a tapered channel. These studies again showed that while a good closure approximation can be obtained, it requires knowledge of the orientation distribution at a set of points within the flow.

Despite these difficulties, there have still been many numerical studies aimed at predicting the orientation state of fiber suspensions in various complex geometries by assuming a one-way coupling between the suspension flow and the fiber orientation state. In these studies, the flow field is assumed to influence fiber orientation, but remains unaffected by the fiber orientation state. For the most part, these studies have been quite successful. For example, VerWeyst and Tucker (1999) used a Galerkin finite element method (FEM) to predict fiber orientation patterns in a variety of injection molded features using the tensor formulation of fiber orientation. They showed that their predictions compared well with experiments when the detailed calculation can be reduced to two spatial dimensions. They also found that 3D calculations were in good qualitative agreement with experimental observations. Olson et al. (2004) determined analytically the mean flow field along the centerline of a tapered channel, neglecting the two-way coupling between the fluid and fiber phase, then used the Fokker–Plank equation to predict the 2D orientation state for the resulting flow. They chose a global rotary diffusion coefficient which models the effect of turbulence on the orientation state by fitting their computations to the experimental data of Ullmar and Norman (1997) and Zhang (1998). Hyensjö et al. (2007) extended the work of Olson et al. (2004) by using single phase CFD modeling to predict the flow field along streamlines of a tapered channel. They used these results to compute the 2D fiber orientation distribution along individual streamlines of the flow in the absence of fiber–fiber interactions and flow–fiber coupling. Parsheh et al. (2006) studied the effect of contraction shape on fiber orientation using a similar approach to that of Olson et al. (2004) where the flow field was approximated analytically and the planar fiber orientation distribution was estimated using a one way coupled solution. These studies showed that fiber orientation is strongly influenced by the shape of the contraction and independent of turbulent dispersion; a result which was attributed to the different flow fields arising inside the different contraction due to different geometries.

The two-way coupling between the flow field and fiber orientation distribution is nonetheless a key element in predicting the behavior of fiber suspensions. In studies by Lipscomb and Denn (1988), the flow of dilute fiber suspensions was compared to that of a pure fluid through an axisymmetric contraction. They modeled fiber orientation by using the so-called aligned fiber approximation, whereby fiber alignment is assumed to be parallel to the streamlines of the flow. These studies showed that structural changes occur in the flow field even for fiber concentrations below 0.1% volume fraction. VerWeyst and Tucker (2002) later used the fully coupled, Galerkin FEM solution to predict the flow of fiber suspensions through a variety of complex geometries which include axisymmetric contractions, expansions and center-gated disks. For the axisymmetric expansion, they showed the formation of a large corner vortex and that this vortex grows in size with increasing fiber concentration. They also showed that the size of the vortex predicted with a coupled solution was much larger than that predicted with an uncoupled solution. For the center-gated disk, they report that the effect of the coupling was to displace streamlines toward the bottom surface as flow enters the disk region, and to align the fibers more rapidly in the radial direction. What is clear from these studies is that there is a significant difference between the coupled and uncoupled solution for the flow field and fiber orientation distribution.

Experimental measurements of suspension flows seem to be far fewer. However, those that do exist suggest that the flow of fiber suspensions differs considerably from the flow of Newtonian fluids, particularly under laminar conditions. For example, Xu and Aidun (2005) experimentally measured the velocity profiles of fiber suspensions in a rectangular channel using pulsed ultrasound Doppler velocimetry. The fiber concentration in their measurements was varied in the range $0.67 \leqslant nL^3 \leqslant 6.7$ and covered Reynolds numbers ranging from 2000 to 92,000. Their velocity profile measurements showed the formation a plug region in the center of the channel for $nL^3 = 6.7$ at $Re = 2000$. They suggest that the plug region may be the result of mechanical entanglement of the fiber phase which results in a fluid/fiber network that flows as a plug. Heath et al. (2007) experimentally studied the flow of a 0.4% mass concentration pulp suspension through a 1:5 axis symmetric sudden expansion. They found that for a mean velocity, $U \approx 0.5$, the suspension moved as a plug far after the expansion, with the exception of a narrow gap near the wall where flow gradients were found to exist.

This current study is motivated by a need to investigate the effect of the two-way coupling on the flow and orientation state of fiber suspensions in a tapered channel. We directly compute the orientation distribution function along individual streamlines of the flow using the rotary diffusion model of Folgar and Tucker (1984), that is Eq. (6) using values for the interaction coefficient, C_I, as previously measured by Krochak et al. (2008). In the first part of this work, we compare flow fields in the contraction predicted with and without the coupling based on two different fiber orientation states at the contraction inlet, namely a partially aligned and a fully random fiber orientation state. That is, we compare the flow of a pure Newtonian fluid to that of a semi-dilute fiber suspension based on different inlet conditions. In the second part of this work, we compare model predictions of the orientation state of the suspension, again based on a coupled and uncoupled solution and two different orientation states at the channel inlet. A discussion of the consequences of working with an uncoupled model and the effect on the flow field and fiber orientation predictions is given.

2. Problem formulation

2.1. Fiber orientation evolution model

The two general methods for modeling the behavior of fibers in suspension are the Lagrangian and Eulerian methods. In the Lagrangian method, the equations of motion for a single fiber are solved for a given velocity field and the process is repeated for each fiber within the suspension. While the Lagrangian method can be quite accurate, it is computationally intensive, particularly for non-dilute suspensions flowing within complex geometries. With the Eulerian method, the probability distribution of fiber orientation (and possibly position) is determined by solving a convection–diffusion equation, namely a Fokker–Plank type equation. With this approach the mean flow field convects the fibers position

and orientation while long range, hydrodynamic fiber–fiber interactions dampen alignment. This dampening, or diffusion-type process effectively results in a flux which opposes the local gradient of the mean fiber orientation state.

The following general assumptions will be made for the Eulerian analysis outlined below:

1. The nominal fiber length is small enough that the flow field can be assumed to be linear along the length of the fiber.
2. The orientation state of the fibers at a point in space can be described by a probability distribution function, Ψ.
3. The fibers are uniformly distributed in space throughout the flow field and translate along streamlines of the flow.
4. Fibers are rigid and large enough that Brownian motion can be neglected.

The linear contraction used in this study is shown in Fig. 2. It consists of a channel bounded both above and below by rigid walls converging at a fixed angle. To further simplify the problem, we consider a 2D planar model of fiber orientation where each fiber is assumed to be oriented in the xy-plane, with an orientation described by the single angle ϕ. This is not actually true in theory, where the rotary diffusion term creates out-of-plane orientation in planar flows. However, the flow field is idealized as planar which implies the fiber orientation in the θ direction will be symmetric about $\theta = \frac{\pi}{2}$ (e.g. Hyensjo and Dahlkild, 2008). Therefore we believe that the effect of the out-of-plane fiber orientation will not significantly change the qualitative behavior of our numerical predictions, and the effect of the two-way coupling will still be well established. As a result of this assumption, the fiber orientation vector in the xy-plane is defined as follows:

$$\mathbf{p} = \begin{bmatrix} \cos\phi \\ \sin\phi \end{bmatrix} \tag{7}$$

In order to directly determine the orientation distribution function in shear flows, a number of authors (e.g. Leal and Hinch, 1971; Folgar and Tucker, 1984; Altan et al., 1989; Koch, 1995; Lin and Zhang, 2002; Parsheh et al., 2005; Alexandrou and Mitsoulis, 2007) describe the evolution of fiber orientation by a probability density function Ψ that obeys a Fokker–Planck relationship, i.e.

$$\frac{\partial\Psi}{\partial t} + u\frac{\partial\Psi}{\partial x} + v\frac{\partial\Psi}{\partial y} = D_r\frac{\partial^2\Psi}{\partial\phi^2} - \frac{\partial\left(\dot{\phi}\Psi\right)}{\partial\phi} \tag{8}$$

where u and v are the fluid velocity field components in the x- and y-directions, respectively, and D_r the rotary diffusion coefficient. To re-iterate, D_r is defined according to Eq. (6) using values of C_I as measured by Krochak et al. (2008). $\dot{\phi}$ in Eq. (8) is the rotational velocity of an individual particle moving in a laminar flow and is modeled according to Jefferey's equation (Jeffery, 1922)

$$\dot{\phi} = \frac{1}{2}\left(\frac{\partial v}{\partial y} - \frac{\partial u}{\partial x}\right)\sin(2\phi) - \frac{\partial u}{\partial y}\sin^2(\phi) + \frac{\partial v}{\partial x}\cos^2(\phi) \tag{9}$$

In general, ϕ can assume any value in the range $-\pi \leqslant \phi \leqslant \pi$. If, however, the fibers are symmetric, as they are assumed to be in this study, the two ends of a fiber are indistinguishable, therefore ϕ can be limited to the range $-\frac{\pi}{2} \leqslant \phi \leqslant \frac{\pi}{2}$. Ψ on the other hand, is free to assume all non-negative, real values. The two extremes of this range are $\Psi = \infty$ and $\Psi = 0$. This extreme case is only possible when the suspension is in a perfectly aligned orientation state, i.e. every fiber in the suspension is aligned in exactly the same direction. In this rare case, Ψ becomes a Dirac delta-function, with its singularity, or infinite value occurring at the value of ϕ corresponding to the direction of fiber alignment, and $\Psi = 0$ for all other values of ϕ.

The boundary conditions for Ψ are as follows:

1. Since the two ends of a fiber are indistinguishable from one another, periodic boundary conditions must be enforced with respect to the orientation angle ϕ, that is

$$\Psi(x, y, \phi) = \Psi(x, y, \phi + \pi) \tag{10}$$

2. Since Ψ is a probability density function it must satisfy a normalization constraint

$$\int_{-\frac{\pi}{2}}^{\frac{\pi}{2}} \Psi(x, y, \phi) = 1 \tag{11}$$

3. At the channel inlet we consider two different inlet fiber orientation states, namely a fully random orientation state which results in a constant value of Ψ, that is

$$\Psi(0, y, \phi) = \frac{1}{\pi} \tag{12}$$

The other inlet orientation state considered is a partially aligned one, where Ψ is set to equal the experimentally observed orientation distribution previously observed by Krochak et al. (2008), that is

$$\Psi(0, y, \phi) = \Psi_{exp}(0, y, \phi) \tag{13}$$

These two inlet conditions are shown in Fig. 3.

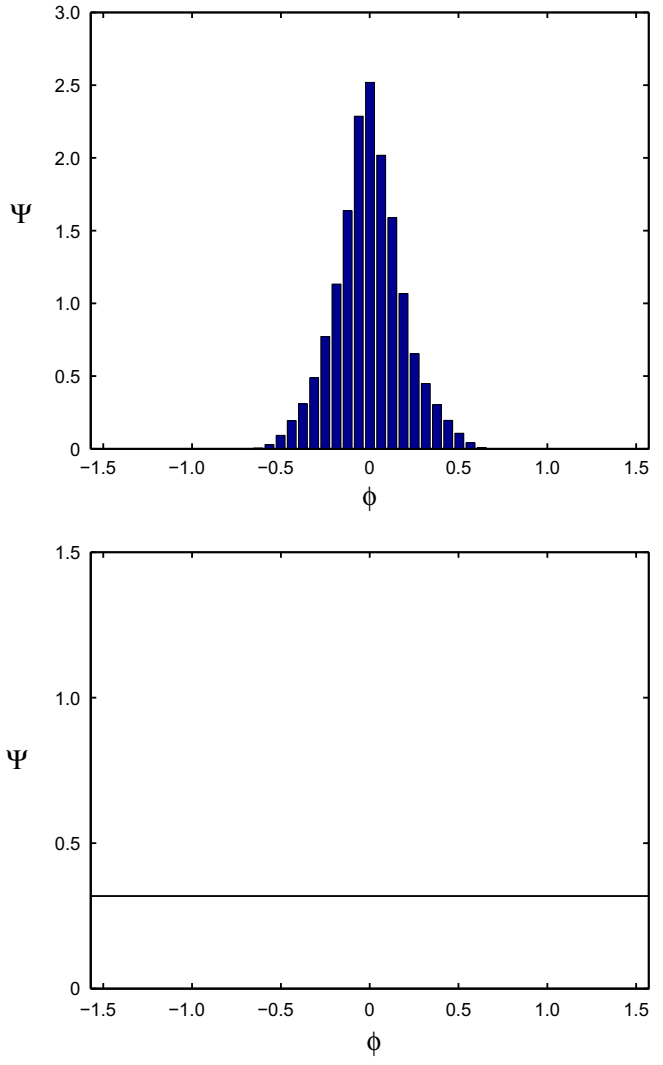

Fig. 3. Plots of the fiber orientation distribution at the contraction inlet. Shown are a partially aligned orientation state (top) and a random orientation state (bottom).

It should be pointed out that no boundary conditions are assigned to Ψ along the walls of the channel. At distances less than one half fiber length from the wall, a rigorous formulation of the problem should account for the fact that fibers are not free to assume all orientation states, since some fiber orientations in this region would place one end of the fiber inside the wall. The near wall depletion of allowed fiber orientation states is also believed to result in a non-uniform fiber concentration profile in this near wall region (e.g. Schiek and Shaqfeh, 1995). This simplification, albeit a common one in fiber orientation modeling, may lead to some errors in the model predictions. For example, it has previously been shown that just outside of this near wall region, fiber orientation shifts away from the channel walls (e.g. Stover and Cohen, 1990; Olson, 1996; Asplund and Norman, 2004; Hyensjö et al., 2007). This shift in fiber orientation near the channel walls may be one of the underlying mechanisms behind structural changes to the flow field and thus to the fiber orientation state when a two-way coupled model is used. In the later stages of the channel used in this work, particularly toward the end of the channel, neglecting these near wall boundary conditions should not result in any significant errors since the fiber suspension becomes highly aligned in a direction parallel to the x-axis. That is, fibers do not assume any of these a-physical orientation states. However, neglecting these boundary conditions in the earlier stages of the channel may have a strong impact on the suspension viscosity and in the momentum transfer, particularly for suspensions entering the channel in a fully random orientation state. We do not consider non-uniform concentration profiles, nor do we impose these rigorous boundary conditions on Ψ near the channel walls in this work. The only physical constraint that is enforced near the channel walls in this work is that Ψ cannot be transported through the walls, that is,

$$u\frac{\partial \Psi}{\partial x} + v\frac{\partial \Psi}{\partial y} = 0 \tag{14}$$

This condition is naturally satisfied by the no-slip constraint of the fluid at the walls given that $\frac{\partial \Psi}{\partial x}$ and $\frac{\partial \Psi}{\partial y}$ remain finite.

The fluid flow is described using Cauchy's equations of motion for an incompressible fluid, that is

$$\nabla \cdot \mathbf{u} = 0 \tag{15}$$

$$\rho\left(\frac{\partial \mathbf{u}}{\partial t} + \mathbf{u}\cdot\nabla\mathbf{u}\right) = -\nabla P + \nabla\cdot\tau \tag{16}$$

where ρ is the fluid density, P is the pressure and τ is the stress tensor, that is the sum of both the Newtonian fluid and fiber contributions

$$\tau = \mu(\nabla\mathbf{u} + \nabla\mathbf{u}^T) + \tau^{\text{fiber}} \tag{17}$$

The fiber stress term, τ^{fiber} couples the presence of the fibers into the momentum equations and depends on the orientation state of the suspension. For this study, we use the form derived by Shaqfeh and Fredrickson (1990) given by Eq. (2).

2.2. Numerical formulation

Numerical computations are carried out for the flow of semi-dilute fiber suspensions of concentration $nL^3 = 8$, or an equivalent volume fraction $c = 0.0025$. The channel geometry is shown in Fig. 2 where we used an inlet height, $y_0 = 0.026$ m, an exit height, $y_e = 0.0026$ m and a channel length, $l = 0.13$ m. This results in a taper angle of 10.2° with respect to the x-axis, and a contraction ratio, that is the ratio inlet to exit heights of the channel, $R = 10$, which is typical of many industrial headboxes. These physical dimensions were ultimately chosen to match a similar experimental device at our research facility from which the interaction coefficient, that is, C_I, in Eq. (6) was measured, along with the experimental inlet conditions for Ψ. For $nL^3 = 8$, Krochak et al. (2008) determined the interaction coefficient to be $C_I = 0.037$.

The flow field is computed in this device using the commercial software package, FLUENT (www.fluent.com). The solution to the flow field is obtained using a 2D, segregated, implicit solver, with water at 20 °C as the fluid phase. A no-slip condition is enforced along the channel walls. At the channel inlet, a parabolic profile is enforced with a peak inlet velocity of 0.01 m/s in the x-direction. It should be pointed out that this choice of boundary condition is not necessarily correct for fiber suspension flows, as the fibers alter the structure and profile of the flow. However, the effect of the fiber phase on the flow field can still be well studied with this choice of boundary condition by means of studying differences between coupled and uncoupled velocity fields further down the channel. An iterative procedure is used whereby the flow field is initially determined for the pure fluid that is water with no fibers, after which Eqs. (8) and (9) are solved using the initial flow field data. The contribution of the fiber phase to the total stress on the fluid is defined by Eq. (2) and is computed upon solving the orientation equations for Ψ. Once computed, the gradient of the fiber stress is determined and then treated as a momentum source term in the fluid momentum equations. This source term is then used in Fluent by means of a so-called User Defined Function written in C and interpreted by Fluent. The fluid flow equations are then solved again to produce a new flow field. On each iteration, the flow field is deemed to be converged when the L_2 norm of the solution residual is less than 10^{-6}. The process is repeated until the change in the L_2 norm of the velocity vector between successive iterations is less than 10^{-6}. Changes in the total pressure were not considered as part of the convergence criterion since they were typically on the order of 10^{-3} between successive iterations.

Eq. (8) is solved along individual streamlines of the flow under steady-state conditions and then the solution is interpolated onto the original 2D rectangular mesh used in solving the flow equations. We placed streamlines at the inlet channel heights $y = \pm 0.0220$, ± 0.0183, ± 0.0147, ± 0.0110, ± 0.0073, ± 0.0037, 0. By solving along individual streamlines of the flow, Eqs. (8) and (9) are reduced to a quasi-1D problem which is formulated as follows. The values of $u, v, \frac{\partial u}{\partial x}, \frac{\partial v}{\partial x}, \frac{\partial u}{\partial y}, \frac{\partial v}{\partial y}$ are computed using Eqs. (15) and (16), and their values are mapped onto each streamline position, $s(x,y)$ using a commercial CFD visualization program, Tecplot (www.tecplot.com). With these values known, $\dot{\phi}(x,y)$ is computed according to Eq. (9) at each Cartesian point, (x,y), along each streamline. The streamline position variable, $s(x,y)$, is computed by integrating the differential arc length of each streamline, beginning at the channel inlet where $s(0,y_0) = 0$, through to the channel exit. More specifically, we define the streamline coordinate as follows:

$$s(x,y) = \int_{(x_o,y_o)}^{(x,y)} \sqrt{dx'^2 + dy'^2} \tag{18}$$

where (x_o, y_o) are the starting points for each individual streamline at the channel inlet and (x', y') are integration variables. Therefore, $s(x,y)$ is the distance along the respective streamline. Eq. (8) is then mapped onto each streamline according to the following transformations:

$$\frac{\partial \Psi}{\partial x} = \frac{\partial \Psi}{\partial s}\frac{\partial s}{\partial x} \tag{19}$$

$$\frac{\partial \Psi}{\partial y} = \frac{\partial \Psi}{\partial s}\frac{\partial s}{\partial y} \tag{20}$$

This leads to the steady-state, quasi-1D form of Eq. (8)

$$u\frac{\partial \Psi}{\partial s}\frac{\partial s}{\partial x} + v\frac{\partial \Psi}{\partial s}\frac{\partial s}{\partial y} = D_r\frac{\partial^2 \Psi}{\partial \phi^2} - \frac{\partial\left(\dot{\phi}(s(x,y))\Psi\right)}{\partial \phi} \tag{21}$$

Eq. (21) is discretized using first-order accurate, implicit forward differences with respect to the spatial streamline variable, s, and second-order accurate centered differences with respect to the orientation angle ϕ. This yields the following system of equations to be solved:

$$\left(u_{i,j}\frac{\partial s}{\partial x_{i,j}} + v_{i,j}\frac{\partial s}{\partial y_{i,j}}\right)\frac{\Psi_{i+1,j} - \Psi_{i,j}}{\Delta s} = D_r\frac{\Psi_{i+1,j+1} - 2\Psi_{i+1,j} + \Psi_{i+1,j-1}}{\Delta\phi^2} - \dot{\phi}_{i,j}\frac{\Psi_{i+1,j+1} - \Psi_{i+1,j-1}}{2\Delta\phi} - \frac{\dot{\phi}}{\Delta\phi_{i,j}}\Psi_{i+1,j} \tag{22}$$

Eq. (22) is solved using a Gauss–Seidel method for each iterative solution of the orientation equations. In general, a total of four iterations of each of the flow field equations, and of the orientation equations were required to obtain a fully converged solution. An example of the convergence of the flow field is shown in Fig. 4.

The mesh used to solve the fluid mass and momentum equations is shown in Fig. 5(a). It consisted of 555 quadrilateral cells and 608 nodes. Each streamline was discretized uniformly using a total of 100 mesh points in the streamline variable, s, and a uniform, 500 point grid was used in ϕ when solving the orientation equations. Mesh independent solutions were obtained in each case. Solutions were compared for Ψ and $\mathbf{u}$ on the 555 cell mesh, with those obtained on fine mesh consisting of 6528 quadrilateral cells and 6708 nodes.

We define the relative solution error for these primary variables as follows. For Ψ, we define the error as

$$\Delta\Psi = \frac{\|\Psi_{\text{Fine}} - \Psi_{\text{Coarse}}\|_2}{\|\Psi_{\text{Fine}}\|_2} \tag{23}$$

and for the velocity field, $\mathbf{u}$,

$$\Delta\mathbf{u} = \frac{\|\mathbf{u}_{\text{Fine}} - \mathbf{u}_{\text{Coarse}}\|_2}{\|\mathbf{u}_{\text{Fine}}\|_2} \tag{24}$$

For the velocity field, we also define the solution difference, $\delta\mathbf{u}$, as follows:

$$\delta\mathbf{u} = |\mathbf{u}_{\text{Fine}} - \mathbf{u}_{\text{Coarse}}| \tag{25}$$

Fig. 6 shows a comparison of the difference in solutions obtained on the two meshes. For the velocity field, we first show the solution difference, $\delta\mathbf{u}$ along each streamline in the upper half of the channel. This is followed by the L_2 norm of the relative difference in solutions along each streamline obtained with the two different mesh sizes. We show only the streamlines for the upper half of the channel, where streamline 1 corresponds to the streamline closest the channel wall, while streamline 7 (C) corresponds to the channel centerline. In the case of the fine mesh, 300 mesh points are used to discretize the streamline variable, s, and the solution obtained on the coarse mesh is interpolated onto the fine mesh in order to make a comparison. For the flow field, (a), we see that $\delta\mathbf{u} \leqslant 0.001$ everywhere except for the streamline closest to the wall and only near the channel exit. Furthermore, the L_2 norm of the relative solution difference is less than 8% in all cases, with the greatest error occurring along the streamline nearest the channel wall.

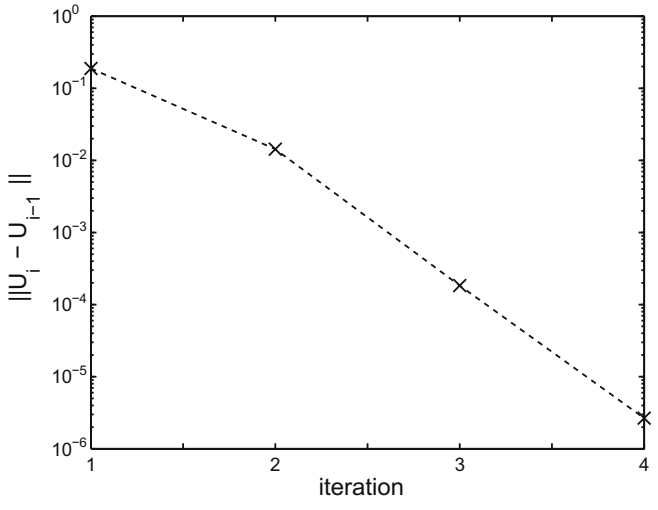

Fig. 4. Plot of the L_2 norm of the relative change in the velocity vector between successive iterations.

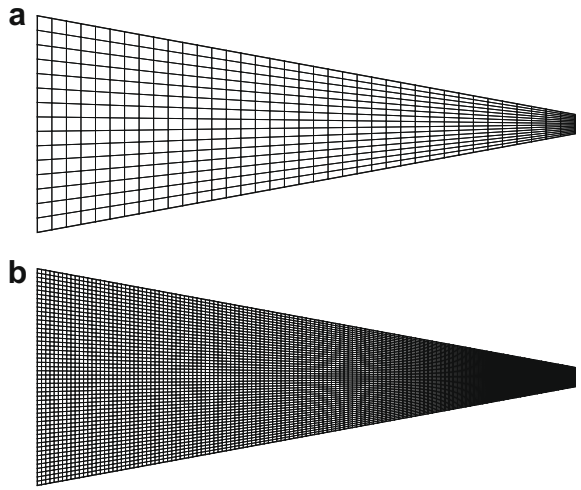

Fig. 5. An example of the mesh used to predict the flow field in the contracting channel (a), and a second mesh used to show mesh convergence (b).

3. Results

In this section, we present numerical predictions of the flow field and fiber orientation distribution for the flow of semi-dilute fiber suspensions with $nL^3 = 8$. All predictions are based on water at 20 °C as the suspending fluid.

3.1. Effect of fiber phase on flow field

We begin the analysis by comparing the predicted velocity fields. Figs. 7 and 8 show plots of the velocity field vectors corresponding to the pure fluid flow and for the suspension flow, respectively. The velocity vectors corresponding to the pure fluid flow is always in the same direction as that of the fiber suspension flow. This result is largely due to the fact that the channel geometry imposes large acceleration on the flow and forces it in one principal direction, namely toward the exit. Since the flow is laminar, accelerating, and bound by a linear taper, no significant directional changes occur in the flow field when the two-way coupling term is included.

The fiber phase does, however, have a significant impact on the flow. A careful examination of the velocity profiles shows that structural changes occur when the fiber phase is considered in the momentum equations. Fig. 9 supports this claim. Here, the velocity in the x-direction of the suspension flow is compared to that of the pure fluid flow along the centerline of the channel. This plot shows that the centerline velocity is always greater for the suspension flows compared to the flow of pure water, and is essentially independent of the fiber orientation state at the channel inlet. For the suspension flow, we argue that the effect of the fiber

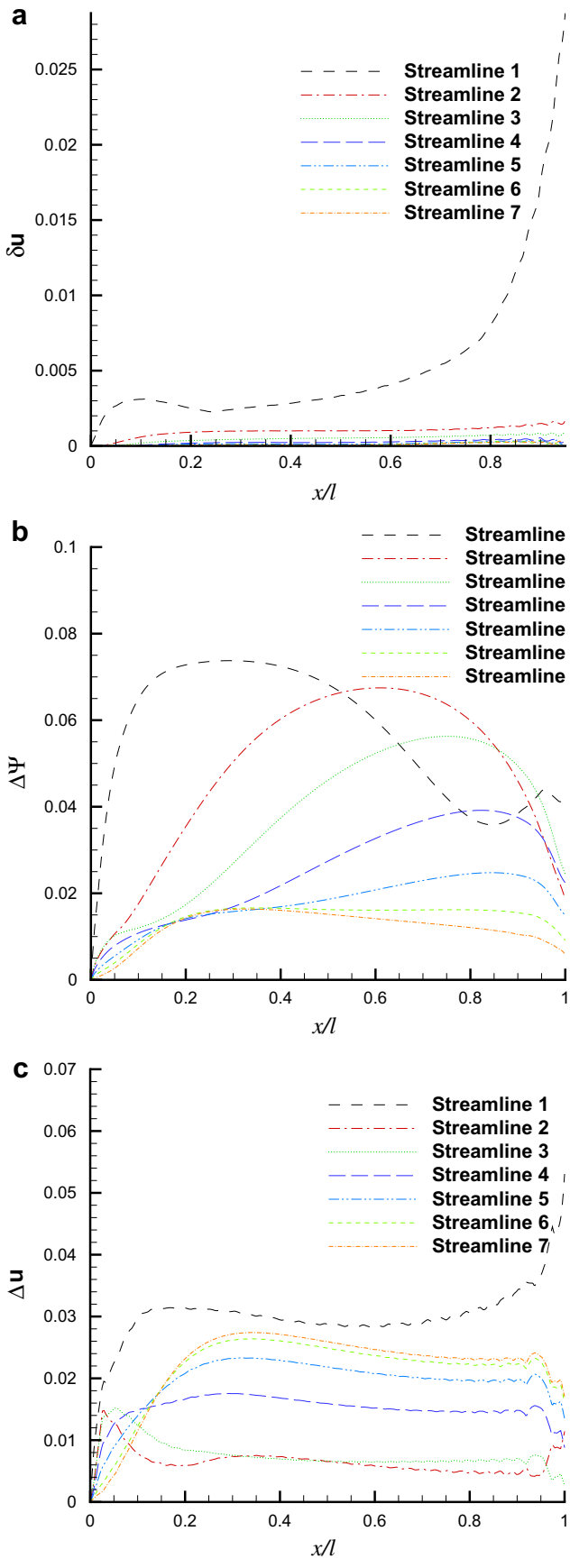

Fig. 6. Comparison of solutions obtained with the two different mesh sizes. A direct comparison of the velocity field solution difference (a), the L_2 norm of the difference in solutions for Ψ (b), and the L_2 norm of the difference in solutions $\mathbf{u}$ (c).

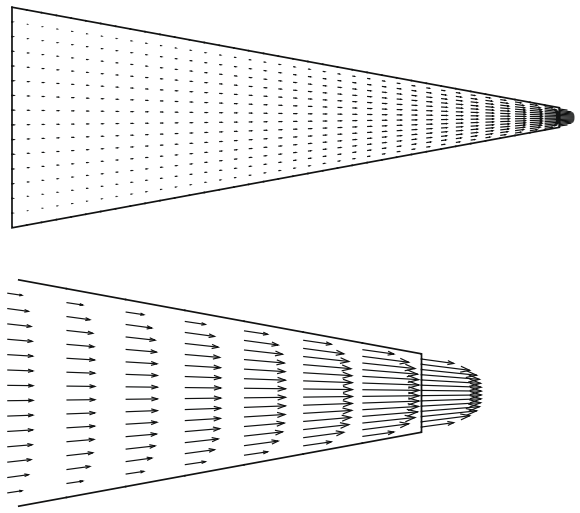

Fig. 7. Vector plots of the velocity field for the flow of water.

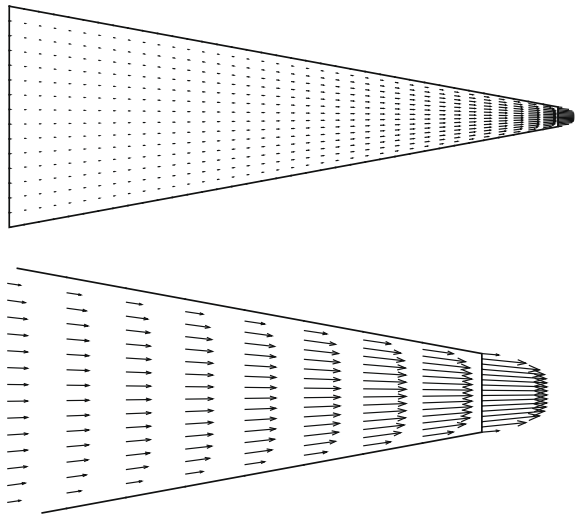

Fig. 8. Vector plots of the velocity field for the suspension flow.

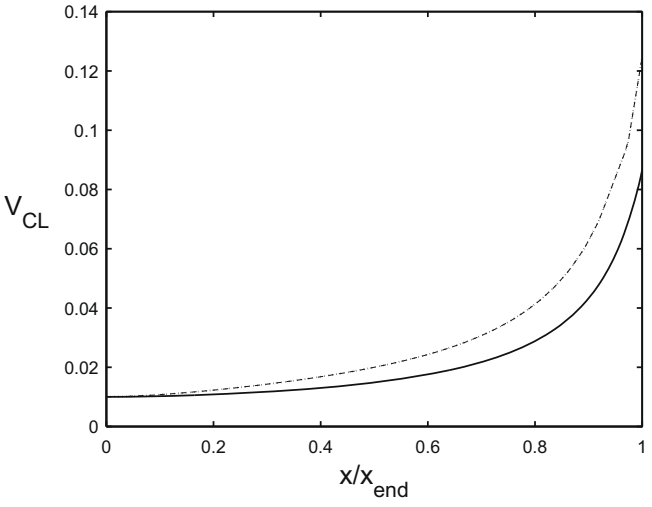

Fig. 9. Comparison of the centerline velocity magnitudes for the flow of the pure fluid, an initially aligned suspension and an initially random suspension.

phase is to redirect the flow near the channel walls toward the middle of the contraction. As will be shown in Section 3.2, near the channel walls, fiber orientation tends to shift away from the walls and toward the middle of the channel. This shift in fiber orientation is believed to redirect the flow toward the middle of the channel resulting in an increased velocity magnitude away from the walls and a suspension that flows faster than would a pure fluid under identical conditions. Generally speaking, this behavior is the same for both the initially aligned and initially random suspension orientation states. This finding may in fact be related to a reduction in near wall shear stress. Reductions in drag associated with turbulent suspension flows have previously been observed by other investigators (e.g. Paschkewitz et al., 2004), however, this phenomenon has not been further studied here.

Structural differences also occur to the flow field across the channel, that is, in the y-direction, for the fiber suspension flow. Fig. 10 shows the velocity magnitude distributions as a function of channel height, y, at several fixed points along the channel length for the initially aligned suspension, the initially random suspension, and for the pure fluid. For the flow of the pure fluid, the highest point of velocity occurs along the channel centerline and decreases to zero along the channel walls, a result which is typical of a laminar Newtonian channel flow. The flow resembles the classic Jeffery–Hamel flow.

However, when the fibers are present, the velocity profiles are significantly different. Near the centerline, the velocity profiles change from having a large degree of curvature to something that is approximately constant across the channel cross-section, that is in the y-direction, except in a small region very close to the wall. To reiterate, it is believed that the fiber phase redirects the flow near the channel walls toward the middle of the contraction, effectively increasing the velocity magnitude around the centerline and creating something that appears to have a plug flow velocity distribution. It should be pointed out that this effect is most notable closer to the channel inlet where a-physical fiber orientation states may arise near the walls. However, since there are no noticeable differences in velocity profiles between the initially aligned and initially random orientation states, the effect of inadequately prescribing boundary conditions on Ψ is thought to be small. These numerical predictions of the velocity profiles are in agreement with the experimental results of Xu and Aidun (2005). However, here, we argue that the plug-type flow profile results from the momentum transfer between the fluid and fiber phases, along with a redirection of flow near the channel walls into the middle of the channel. Similar numerical predictions have been made by Lin et al. (2007) in studying the flow of turbulent fiber suspensions through a converging channel. They too showed that significant structural changes to the mean velocity profile occur when the fiber phase is considered. However, they found a decrease in the centerline velocity along with a significant increase in the velocity near the channel walls. Other attempts at modeling the flow of fiber suspensions using non-Newtonian stress models have seen limited success. For example, Duffy (2003) reviewed several attempts at using non-Newtonian models such as shear thinning and thickening, Bingham plastic, and friction factor-Reynolds number method and showed that none of these models were suitable when describing fiber suspension flow. Duffy (2003) proposed several mechanistic based models, however, these models relied on empirical correlations in order for them to be successful. It would certainly make for interesting future work to confirm the numerical predictions made in this work with experimental measurements.

Another point of interest is to compare the effect of the fibers on the streamlines of the flow. Comparing the streamlines is particularly important for streamline solution techniques to the fiber orientation problem (e.g. Poitou et al., 2000; Chiba and Nakamura, 1998), such as the method used in this work, as well as in the so-called

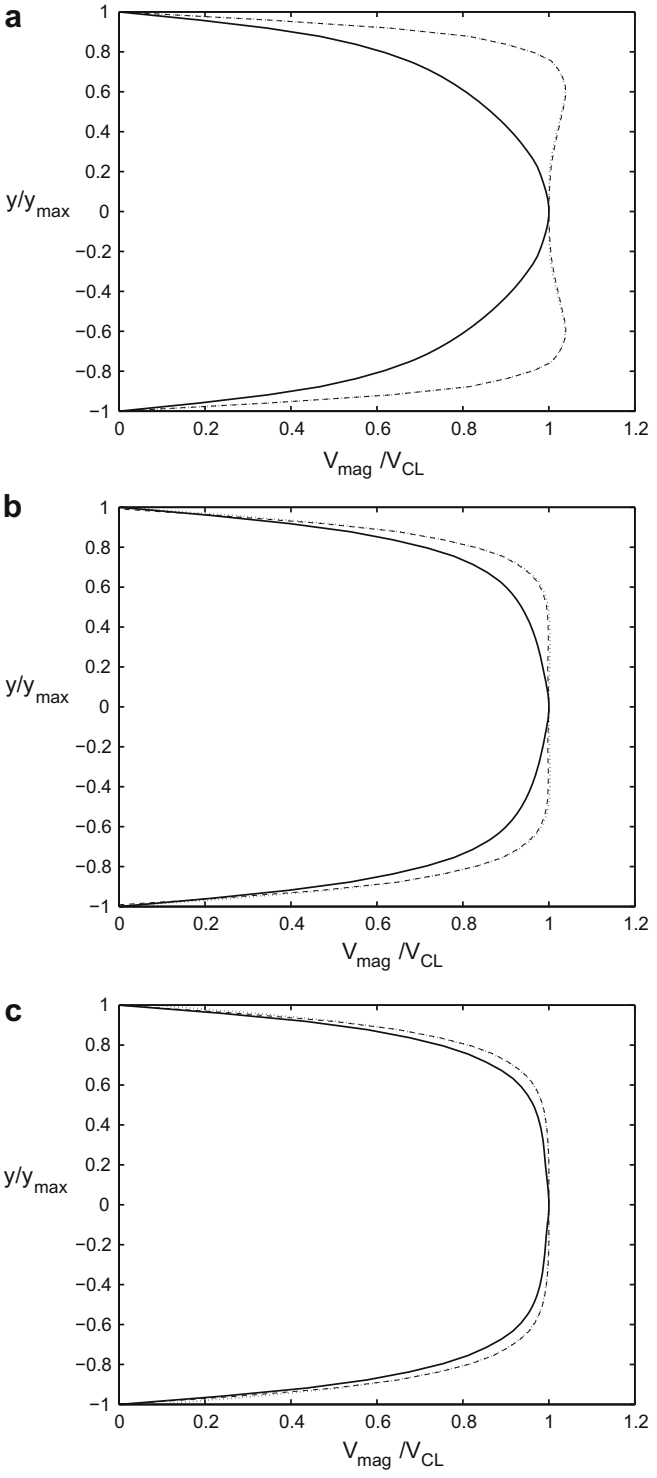

Fig. 10. Comparison of the velocity magnitudes of the initially aligned suspension (·····), the initially random suspension (------) and the pure fluid (———) vs. channel height at (a) $x/x_{end} = 0.3$, (b) $x/x_{end} = 0.6$ and (c) $x/x_{end} = 0.95$.

aligned fiber approximation. In the aligned fiber approximation, fiber alignment is assumed to be parallel to the streamlines of the flow (e.g. Lipscomb and Denn, 1988). While both techniques can be quite accurate for certain flow fields, it is obviously critical to accurately predict the streamlines. Fig. 11 shows a comparison of the predicted location of the streamlines. To re-iterate, we place streamlines at the inlet channel heights of $y = \pm 0.0220$, ± 0.0183, ± 0.0147, ± 0.0110,

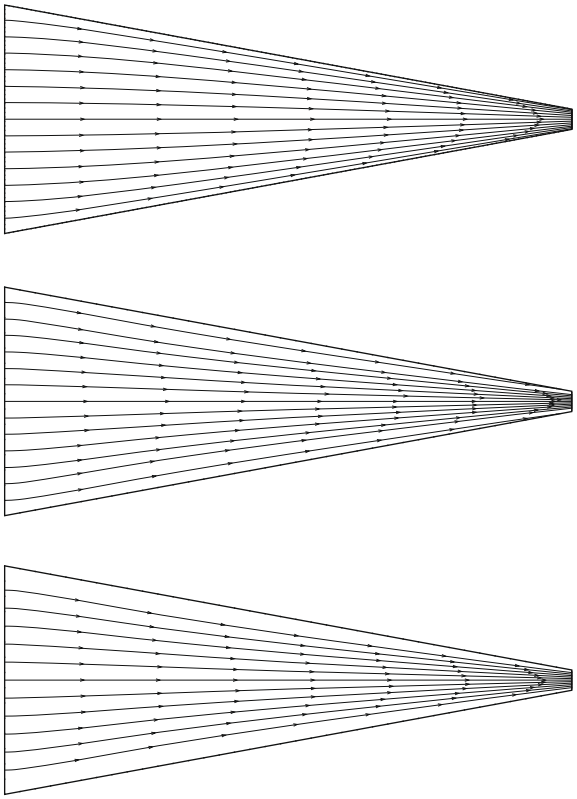

Fig. 11. Comparison of streamlines for the flow of pure water (top), for the partially aligned suspension (middle) and for the initially random suspension (bottom).

±0.0073, ±0.0037, 0. The most notable differences in the streamlines is that for the suspension flow, the streamlines become considerably closer to each other, again supporting the notion that the fibers effectively redirect the flow toward the middle of the channel. This is most obvious by comparing the streamlines closest to the channel walls. For the pure fluid, we see that the streamlines originating closest to the walls, i.e. those originating at $y = \pm 0.0220$, come very close and parallel to the walls. It should be noted that although the streamlines appear to touch the wall, this is in fact not correct – it is a reproduction problem. These same streamlines in the suspension flow are also parallel to the walls, however, they maintain a greater distance from the wall and do so much farther along the channel length. For the initially random suspension, the streamlines maintain this increased distance from the wall through to the channel exit. Further, there is a noticeable curvature to the streamlines associated with the pure fluid, particularly near the channel inlet. This curvature is far less obvious in the streamlines associated with the suspension flow. The streamlines associated with the initially random suspension show the least curvature and are closer to each other compared with the initially aligned suspension. This is again most obvious by noting the large gap between these streamlines and the wall in the initially random suspension. It should be mentioned that the asymmetry in the y-direction corresponding to the partially aligned suspension is likely the result of an asymmetry in the measured orientation distribution at the contraction inlet, see Fig. 3.

3.2. Orientation distribution

Here we look at the effect of the two-way coupling on the orientation distribution function. Before proceeding to the main findings of this section, it is instructive to characterize the evolution of the orientation distribution of interacting fibers along the channel length. Fig. 12 shows the evolution of Ψ along the channel centerline, and along one upper and one lower streamline. The key observation that can be made is that the fiber orientation is most random-like at the channel inlet and becomes increasingly aligned

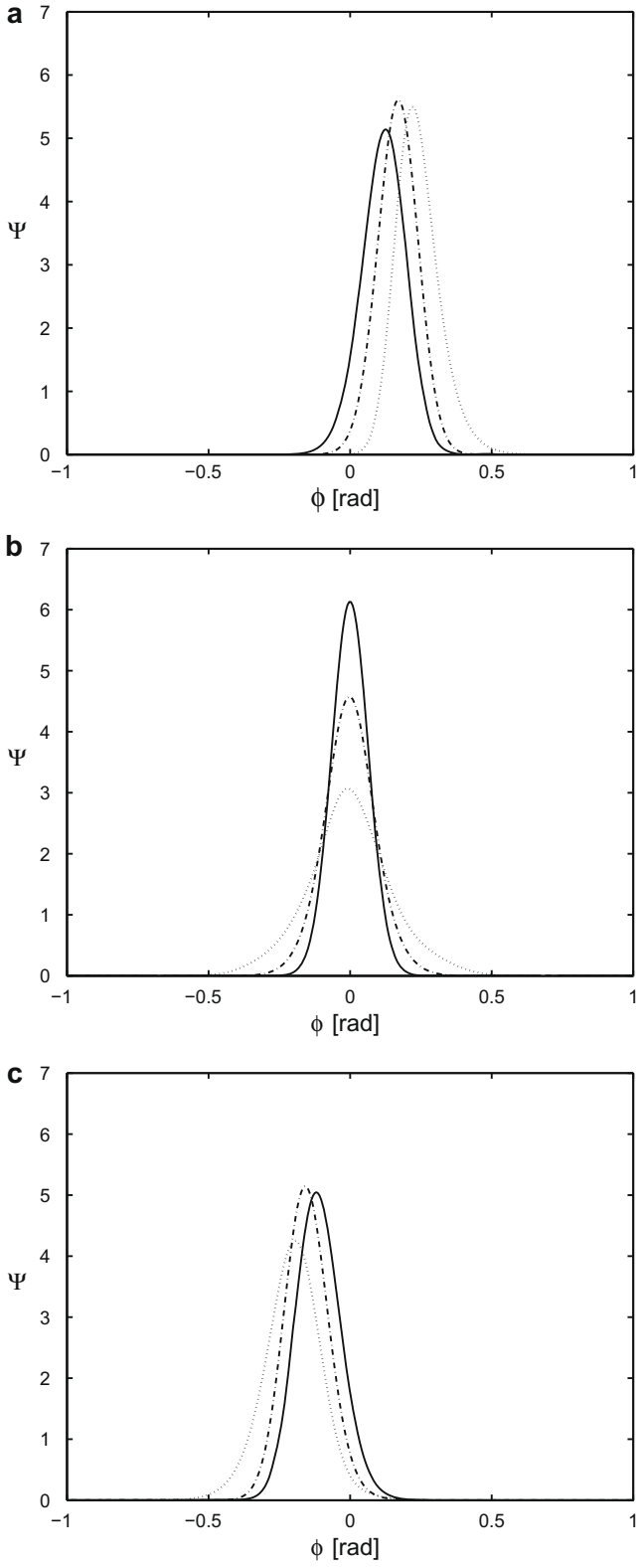

Fig. 12. Development of the orientation distribution along three streamlines of the flow, one in the lower half of the channel (a), one along the central streamline (b) and one in the upper half of the channel (c). The data are given at $\frac{x}{l} = 0.33$ (·····), $\frac{x}{l} = 0.66$ (-·-·-·-·-·-) and $\frac{x}{l} = 1.0$ (———).

in the streamline direction toward the channel exit. This behavior is most obvious along the central streamline and is typical of all cases simulated. From the non-centerline streamline plots, it can be seen that the fiber orientation distribution is clustered about the streamline direction near the inlet and shifts toward the centerline direction near the contraction exit. That is, fibers become highly aligned near the exit in a direction parallel to the x-axis.

In order to better visualize and interpret the orientation distribution over the entire xy-plane we plot the vectors indicating the principal direction of fiber alignment. The principal direction of fiber alignment, $\overline{\mathbf{p}}$, is defined as the eigenvector associated with the largest eigenvalue of the second-order orientation tensor, $\langle \mathbf{pp} \rangle$, where $\langle \mathbf{pp} \rangle$ is defined as

$$\langle \mathbf{pp} \rangle = \int p_i p_j \Psi(\phi)\, d\phi \tag{26}$$

Fig. 13 compares field plots of $\overline{\mathbf{p}}$ obtained with and without the two-way coupling for the fiber suspension entering the channel in a pre-aligned orientation state. The general trend is for fibers to align parallel to streamlines, that is, in the principal direction of the acceleration of the flow. This same trend is found for solutions obtained with and without the coupling, however, the streamlines and streamline directions are not identical when the two-way coupling term is included. As was previously discussed in Section 3.1, the streamlines predicted when the two-way coupling term is included are not exactly the same as those predicted without the coupling, where the later tend to show a fair amount of curvature when compared to the former.

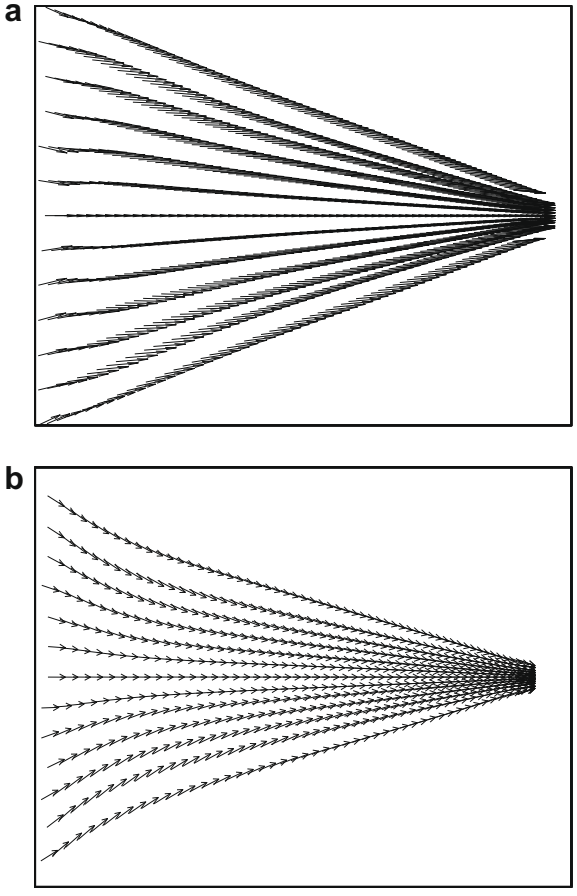

Fig. 13. Comparison of the principal direction of fiber alignment for the initially aligned suspension predicted with two-way coupling (a) and without two-way coupling (b).

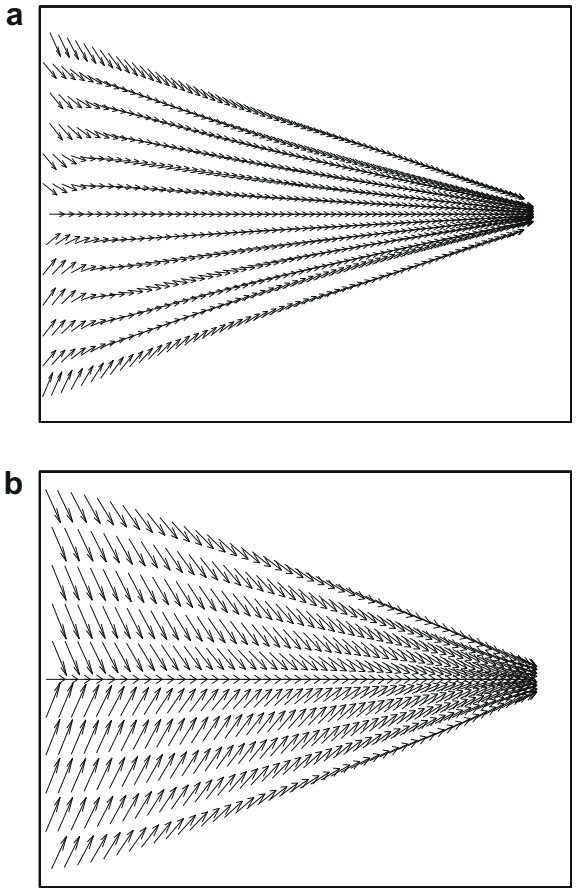

Fig. 14. Comparison of the principal direction of fiber alignment for the initially random suspension predicted with two-way coupling (a) and without two-way coupling (b).

Fig. 14 compares field plots of $\overline{\mathbf{p}}$ obtained with and without the two-way coupling for the fiber suspension entering the channel in a random orientation state. The situation here is quite different. When the suspension enters the channel in a random orientation state, we can see that, when the two-way coupling is accounted for, the suspension aligns in the streamline direction after only a short distance down the channel, i.e. near the point $x = 20$ mm. However, when the two-way coupling is not included, the suspension is predicted to become fully aligned very close to the exit, i.e. near the point $x = 120$ mm. This is of particular importance when modeling industrial headbox flows in papermaking, since fiber suspensions entering a headbox are typically assumed to be fully random in orientation state. Furthermore, many numerical studies of fiber orientation in the headbox assume fibers enter in a fully random orientation state (e.g. Olson et al., 2004; Parsheh et al., 2006; Hyensjö et al., 2007; Hyensjo and Dahlkild, 2008) and knowing how quickly a pulp suspension aligns in the headbox nozzle could be critical to its design.

To fully characterize the fiber orientation distribution in the channel, we define a measure of the degree of fiber alignment about the principal direction of orientation, A_ϕ. A value of A_ϕ equal to unity corresponds to a perfectly aligned suspension, and when $A_\phi = 0.5$, the suspension is in a fully random, or uniform orientation state. A_ϕ can analogously be thought of as a measure of the orientation anisotropy for the suspension. We define A_ϕ mathematically as follows:

$$A_\phi^{th} = \int_{-\frac{\pi}{2}}^{\frac{\pi}{2}} \Psi \cos^2\phi \, d\phi \tag{27}$$

Profiles of A_ϕ with respect to channel height are compared using coupled and uncoupled models at three discrete points along the channel length. Shown in Fig. 15 is a comparison of the pre-aligned suspension flow. For the most part, A_ϕ is not significantly altered when the two-way coupling is included in the calculations. Fig. 15 does, however, show some subtle differences, namely that A_ϕ is slightly overestimated, and somewhat more constant across the channel when the two-way coupling is not included. These small differences are not believed to have to be significant for this

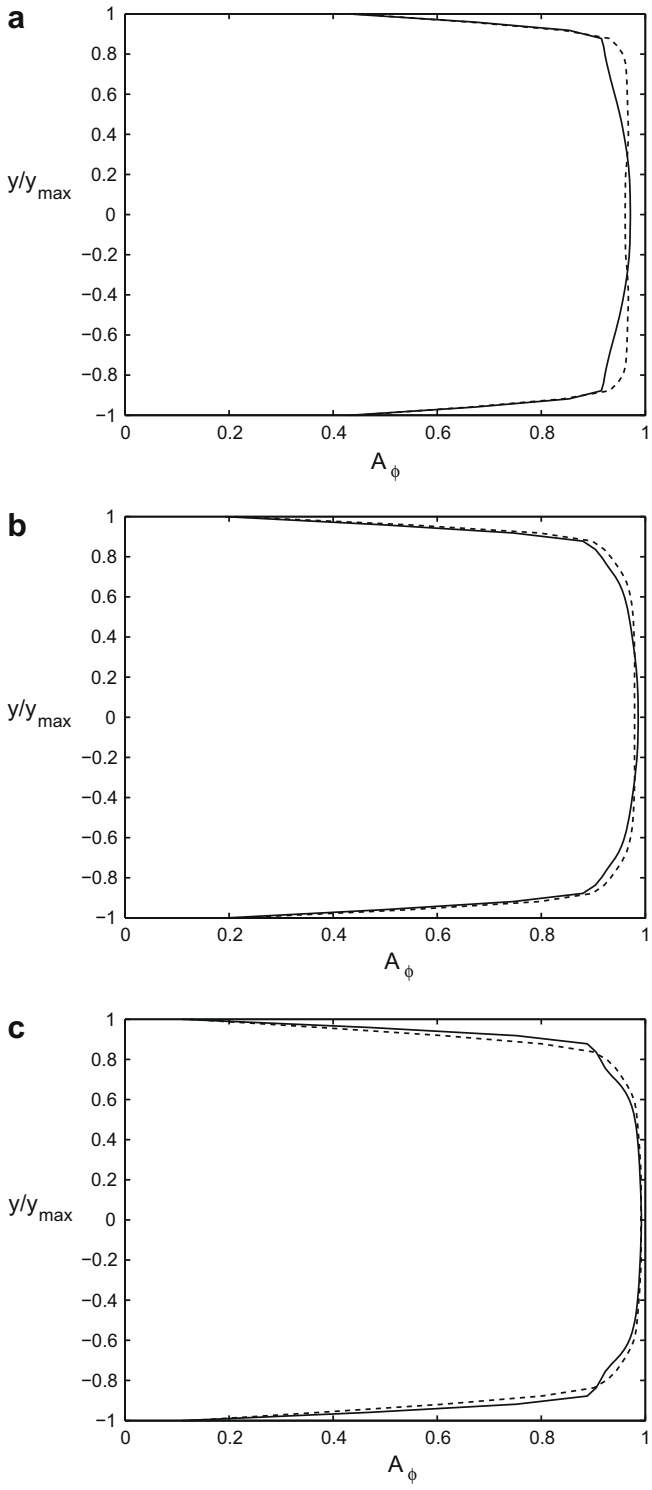

Fig. 15. Comparison of the predicted orientation anisotropy vs. channel height for solutions obtained with and without the two-way coupling at fixed position along the channel length for the initially aligned suspension. The profiles shown correspond to (a) $x/x_{end} = 0.3$, (b) $x/x_{end} = 0.6$ and (c) $x/x_{end} = 0.95$.

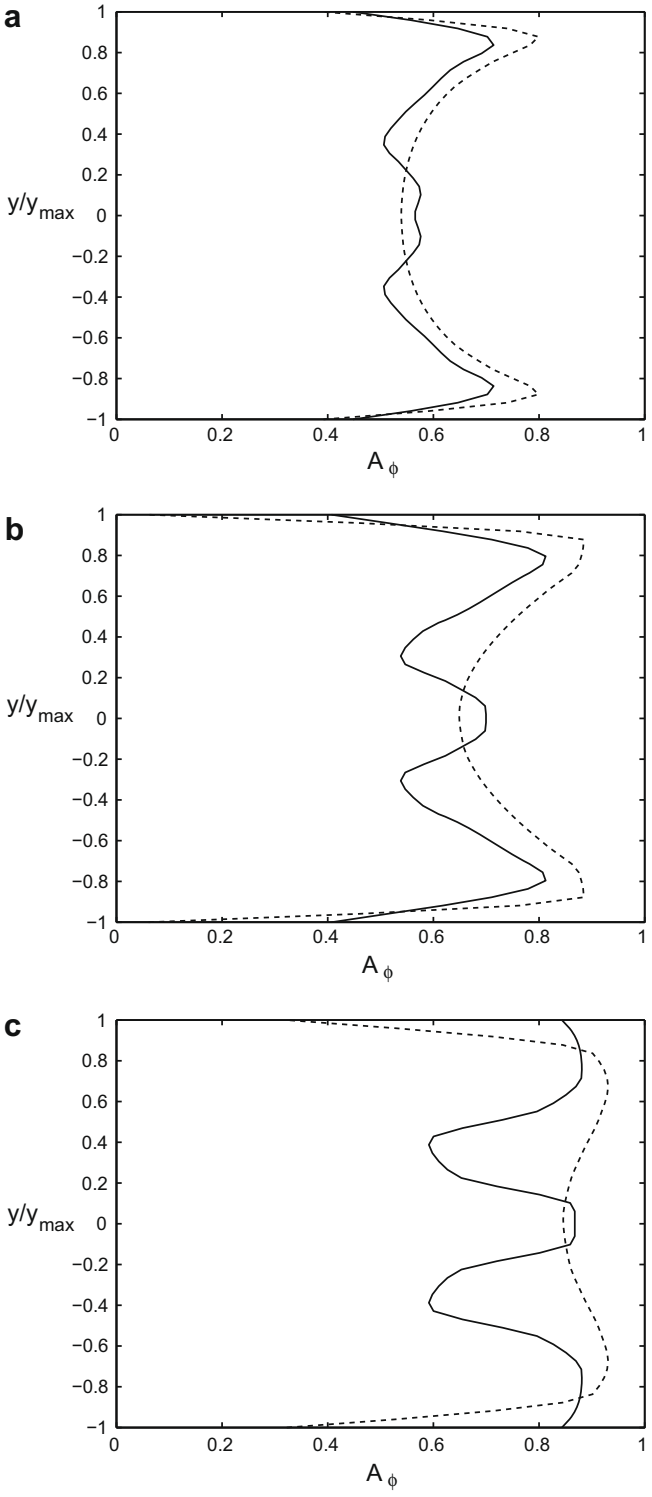

Fig. 16. Comparison of the predicted orientation anisotropy vs. channel height for solutions obtained with and without the two-way coupling at fixed position along the channel length for the initially random suspension. The profiles shown correspond to (a) $x/x_{end} = 0.3$, (b) $x/x_{end} = 0.6$ and (c) $x/x_{end} = 0.95$.

particular flow field, channel geometry and inlet fiber orientation state, however, should still be considered when working with an uncoupled model of fiber orientation.

Fig. 16 shows this same comparison for the suspension which enters the channel in a fully random orientation state. In this case, the orientation anisotropy predicted with and without the two-way coupling is again quite different for an initially random orientation state. Not only is the magnitude of A_ϕ significantly different across the channel, but its character has been significantly changed as well, particularly near the channel centerline.

4. Conclusion

The flow and orientation state of semi-dilute rigid fiber suspensions has been modeled for laminar flow inside a tapered channel using the constitutive model of Shaqfeh and Fredrickson (1990). The model accounts for the two-way interaction between the flow field and fiber orientation state where the flow field influences fiber orientation and the fiber orientation state simultaneously affects the flow field. Long range hydrodynamic fiber–fiber interactions have been included in the model using experimentally determined values for the interaction coefficient. Two different fiber orientation states at the channel inlet are considered, one a partially aligned orientation state, the other, a random orientation state.

The effect of the fiber phase on the flow field is shown to be significant regardless of fiber orientation at the inlet. It is argues that the fiber phase redirects the flow from the channel walls toward the middle of the channel, changing the velocity profile from the standard, laminar, Newtonian channel flow, to something resembling a plug type flow. The fiber phase is also shown to alter the location and direction of the streamlines across the channel length. For the flow of a pure Newtonian fluid, the streamlines display curvature, and remain well separated from one another. However, for the suspension flow, the streamlines lose their curvature and become highly linear and more closely packed to each other. This effect is most pronounced when the suspension enters the channel in a random orientation state.

Including the two-way coupling has a small effect on fiber orientation predictions in the channel, particularly when the suspension enters the channel in a aligned orientation state. In this case, the principal direction of fiber orientation remains parallel to the streamlines. However, in the uncoupled case, this could prove to give false predictions of fiber orientation since the streamline position and direction change in response to the two-way coupling. The effect of the two-way coupling on fiber orientation anisotropy is also small for this case, but not believed to be significant. A significant difference was found when the suspension enters the channel with a random orientation state. In this case, it was shown that when the coupling term is not included, the suspension does not align nearly as fast in the streamline direction, as predicted when the two-way coupling is accounted for. The orientation anisotropy was also shown to be significantly different for the initially random suspension, both quantitatively and qualitatively, when the two-way coupling is included. These findings would suggest the two-way coupling plays a fundamental role in predicting both the flow field and fiber orientation state for the flow of suspension with a random inlet orientation state.

Acknowledgements

Financial support of the Natural Sciences and Engineering Research Council (NSERC) and the Advanced Papermaking Initiative (API) is gratefully acknowledged.

References

Advani, S.G., Tucker, C.L., 1987. The use of tensors to describe and predict fibre orientation in short fibre composites. J. Rheol. 31, 751–784.
Advani, S.G., Tucker, C.L., 1990. Closure approximations for three-dimensional structure tensors. J. Rheol. 34, 367–387.
Alexandrou, A., Mitsoulis, E., 2007. Transient planar squeeze flow of semi-concentrated fiber suspensions using the Dinh–Armstrong model. J. Non-Newton. Fluid Mech. 146, 114–124.
Altan, M.C., Advani, S.G., Güceri, S.I., Pipes, R.B., 1989. On the description of the orientation state for fiber suspensions in homogeneous flows. J. Rheol. 33, 1129–1155.
Asplund, G., Norman, B., 2004. Fibre orientation profile over the thickness of a headbox jet nordic. J. Pulp Paper Sci. 30, 217–221.
Batchelor, G.K., 1970. Slender-body theory for particles of arbitrary cross-section in Stokes flow. J. Fluid Mech. 44, 419–440.
Chiba, K., Nakamura, K., 1998. Numerical solution of fiber suspension flow through a complex channel. J. Non-Newton. Fluid Mech. 78, 167–185.
Chung, D.H., Kwon, T.H., 2001. Improved model of orthotropic closure approximation for flow induced fiber orientation. Polym. Compos. 22, 636–649.
Cintra, J.S., Tucker, C.L., 1995. Orthotropic closure approximations for flow-induced fiber orientation. J. Rheol. 39, 1095–1122.
Cox, R.G., 1970. The motion of long slender bodies in a viscous fluid. J. Fluid Mech. 44, 791–810.
Dinh, S.M., Armstrong, R.C., 1984. A rheological equation of state for semi-concentrated fibre suspensions. J. Rheol. 28, 207–227.
Doi, M., Edwards, S.F., 1984. The Theory of Polymer Dynamics. Oxford University Press, New York.
Duffy, G.G., 2003. The significance of mechanistic-based models in fibre suspension flow nordic. J. Pulp Paper Sci. 18, 74–80.
Folgar, F., Tucker, C.L., 1984. Orientation behavior of fibers in concentrated suspensions. J. Reinf. Plast. Comp. 3, 98–119.
Heath, H.S., Olson, J.A., Buckley, K.R., Lapi, S., Ruth, T.J., Martinez, D.M., 2007. Visualization of the flow of a fibre suspension through a sudden expansion using PET. AIChE J. 53, 327–334.
Hyensjo, M., Dahlkild, A., 2008. Study of the rotational diffusivity coefficient of fibers in planar contracting flows with varying turbulence levels. Int. J. Multiphase Flow 34, 894–903.
Hyensjö, M., Dahlkild, A., Krochak, P., Olson, J., 2007. Modeling the effect of shear flow on fiber orientation anisotropy in a planar contraction. Nord. Pulp Paper Res. J. 22, 376–382.
Jackson, W.C., Advani, S.G., Tucker, C.L., 1985. Predicting the orientation of short fibers in thin compression moldings. J. Comput. Mater. 20, 539–557.
Jeffery, G.B., 1922. The motion of ellipsoidal particles immersed in a viscous fluid. Proc. Roy. Soc. Lond. A 102, 161–179.
Koch, D.L., 1995. A model for orientational diffusion in fibre suspensions. Phys. Fluids 7, 2086–2088.
Krochak, P.J., Martinez, D.M., Olson, J.A., 2008. The orientation of semi-dilute rigid fibre suspensions in a linearly contracting channel. Phys. Fluids 20. doi:10.1063/1.2949277.
Leal, L.G., Hinch, E.J., 1971. The effect of weak brownian rotations on particles in shear flow. Chem. Eng. Commun. 108, 381–401.
Lin, J., Zhang, L., 2002. Numerical simulation of orientation distribution function of cylindrical particle suspensions. Appl. Math. Mech. 23, 906–912.
Lin, J.Z., Zhang, S.L., Olson, J.A., 2007. Effect of fibers on the flow property of turbulent fiber suspensions in a contraction. Fibers Polym. 18, 60–65.
Lipscomb, G.G., Denn, M.M., 1988. Flow of fibre suspensions in complex geometries. J. Non-Newton. Fluid Mech. 26, 297–325.
Olson, J.A., 1996. The effect of fibre length on passage through narrow apertures, Doctoral Thesis, University of British Columbia, Vancouver, Canada.
Olson, J.A., Frigaard, I., Chan, C., Hämäläinen, J.P., 2004. Modeling a turbulent fibre suspension flowing in a planar contraction: the one-dimensional headbox. Int. J. Multiphase Flow 30, 51–66.
Parsheh, M., Brown, M.L., Aidun, C.K., 2005. On the orientation of stiff fibers suspended in a turbulent flow in a planar contraction. J. Fluid Mech. 545, 245–269.
Parsheh, M., Brown, M.L., Aidun, C.K., 2006. Variation of fiber orientation in turbulent flow inside a planar contraction with different shapes. Int. J. Multiphase Flow 32, 1354–1369.
Paschkewitz, J.S., Yves, D., Dimitropoulos, C.D., Shaqfeh, E.S., Parviz, M., 2004. Numerical simulation of turbulent drag reduction using rigid fibers. J. Fluid Mech. 518, 281–317.
Poitou, A., Chinesta, F., Torres, R., 2000. Numerical simulation of the steady recirculating flows of fiber suspensions. J. Non-Newton. Fluid Mech. 90, 65–80.
Rahnama, M., Koch, D.L., Shaqfeh, E.S.G., 1995. The effect of hydrodynamic interactions on the orientation distribution in a fibre suspension subject to simple shear flow. Phys. Fluids 7, 487–506.
Schiek, R.L., Shaqfeh, E.S.G., 1995. A non-local theory for stress in bound. Brownian suspensions of slender, rigid fibers. J. Fluid Mech. 296, 271–324.
Shaqfeh, E.S.G., Fredrickson, G.H., 1990. The hydrodynamic stress in a suspension of rods. Phys. Fluids A 2, 7–24.
Stover, C.A., Cohen, C., 1990. The motion of rodlike particles in the pressure-driven flow between two flat plates. Rheol. Acta 29, 192–203.

Ullmar, M., Norman, B., 1997. Observation of fibre orientation in a headbox nozzle at low consistency. In: TAPPI Proceedings, Engineering and Papermaking Conference, pp. 865–873.

VerWeyst, B.E., Tucker, C.L., 1999. Fibre orientation in 3-D injection molded features: prediction and experiment. Int. Polym. Process. 4, 409–420.

VerWeyst, B.E., Tucker, C.L., 2002. Fibre suspensions in complex geometries: flow/fibre coupling. Can. J. Chem. Eng. 80, 1093–1106.

Xu, H.J., Aidun, C.K., 2005. Characteristics of fiber suspension flow in a rectangular channel. Int. J. Multiphase Flow 31, 318–386.

Zhang, X., 1998. Fibre orientation in a headbox, Masters Thesis, The University of British Columbia, Vancouver, Canada.